ChemComm

Bottom-up formation of gold truncated pyramids smaller than 10 nm on SrTiO3 nanocubes: An application to plasmonic water oxidation

Journal:	*ChemComm*
Manuscript ID	CC-COM-05-2021-002813
Article Type:	Communication

COMMUNICATION

Bottom-up formation of gold truncated pyramids smaller than 10 nm on $SrTiO_3$ nanocubes: An application to plasmonic water oxidation

Received 00th January 20xx,
Accepted 00th January 20xx

DOI: 10.1039/x0xx00000x

Kota Kurokawa,[a] Musashi Fujishima,[b] Shin-ichi Naya,[c] and Hiroaki Tada[a,b*]

Atomically commensurate interface gives rise to Au truncated pyramids < 10 nm on single-crystalline $SrTiO_3$ nanocubes in a simple deposition-precipitation process without surface modifier, and the resulting hybrid nanocrystals exhibit a high level of photocatalytic activity for plasmonic oxygen evolution reaction at light wavelength (λ_{ex}) ≤ 1200 nm.

Downsizing gold (Au) below 10 nm induces high catalytic activity for various important chemical reactions, whereas it is inactive in the bulk state.[1] The activity of Au nanoparticle (NP)-based catalysts and photocatalysts strongly depends also on the shape because the sharp edges and corners of faceted Au NPs can be catalytically active sites.[2-4] In general, reducing Au particle size tends to yield non-faceted spherical Au NPs to lower the total surface energy. The synthesis of faceted Au NPs usually needs habit modifiers strongly adsorbed on the surface, but the particle size is much larger than 10 nm.[5-7] Thus, the development of the technique for synthesizing clean faceted Au NPs smaller than 10 nm is highly required for the applications to (photo)catalysts. On the other hand, Au NP-loaded semiconductor (Au/semiconductor) plasmonic photocatalysts driven by the excitation of Au NPs have recently attracted much interest as a hopeful solar-to-fuel convertor because of the wide spectral response. In the typical Au/TiO_2 system, excitation of the localized surface plasmon resonance (LSPR) of Au NPs generates hot electrons and holes,[8] and part of the hot electrons can be injected into the conduction band (CB) of semiconductor[9,10] to cause a reduction reaction, while the holes left in the Au NP oxidize water. Oxygen evolution reaction (OER) by an $Au/SrTiO_3$ plasmonic photocatalyst was reported to proceed via the interband transition of Au NPs under irradiation by photons with energy ($\hbar\omega$) > ~2 eV (or λ_{ex} < ~600 nm).[11] As such, it is necessary for the efficient solar-to-chemical conversion to simultaneously enhance the efficiency of each elemental step in the plasmonic reaction involving light harvesting by plasmonic metal, hot-carrier generation, hot-electron injection, charge separation, and surface redox reaction,[12] particularly at λ_{ex} > ~600 nm. So far, the material design for the components of the plasmonic photocatalysts has mainly been studied. The activity for OER increases with decreasing Au particle size due to the enhancement in the electrocatalytic activity.[13,14] The shape of Au NP is also an important factor, e.g., Au nanorod/TiO_2 plasmonic photocatalysts have been reported to show high activities for OER [15] and water splitting.[16] Further, the activity depends on the kind of semiconductors.[17,18] The coming major subject in the plasmonic photocatalysts is to devise a simple and feasible methodology for the simultaneous enhancement of the efficiencies of each elemental step.

Here we show that atomically commensurate junction formed by a simple deposition precipitation method can induce faceting of Au NPs to yield clean truncated pyramids < 10 nm on single-crystal $SrTiO_3$ nanocubes with the {100} facets ($Au//SrTiO_3$ NCs, // denotes heteroepitaxial junction). The nanohybrids have been shown to exhibit a high level of activity

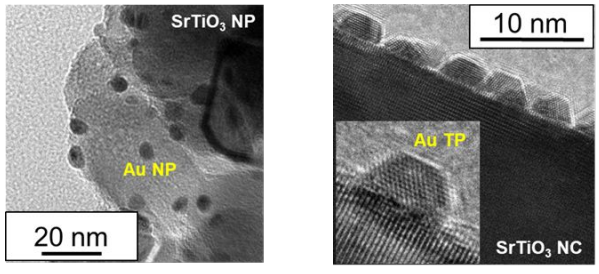

Fig. 1. (A) TEM images of $Au/SrTiO_3$ NPs (A) and $Au/SrTiO_3$ NCs.

[a] *Graduate School of Science and Engineering, Kindai University, 3-4-1, Kowakae, Higashi-Osaka, Osaka 577-8502, Japan.*
[b] *Faculty of Science and Engineering, Kindai University, 3-4-1, Kowakae, Higashi-Osaka, Osaka 577-8502, Japan..*
[c] *Environmental Research Laboratory, Kindai University, 3-4-1, Kowakae, Higashi-Osaka, Osaka 577-8502, Japan.*
Fax: +81-6-6727-4301; Tel:+81-6-6721-2332; E-mail: h-tada@apch.kindai.ac.jp
Electronic Supplementary Information (ESI) available: [details of any supplementary information available should be included here]. See DOI: 10.1039/x0xx00000x

for OER under visible-to-near infrared light (λ_{ex} ≤ 1200 nm). $SrTiO_3$ NCs were synthesized by a hydrothermal method (ESI), and commercially available $SrTiO_3$ NPs (Aldrich) were also used for comparison. In the SEM image of $SrTiO_3$ NPs (Fig. S1A), irregular shaped NPs with the size < 100 nm are observed, while the synthesized sample consists of cubes with a mean size (d_{STO}) of 180 nm (Fig. S1B). In each XRD pattern (Fig. S1C), diffraction peaks are observed at 32.42º, 39.99 º, 46.48 º and 57.80 º which are in agreement with the values for the diffraction from the (110), (111), (200), and (211) planes of $SrTiO_3$, respectively. The distinct and regular spots in the selected area electron diffraction (SAED) pattern of the $SrTiO_3$ NCs verify that the $SrTiO_3$ NC is single crystalline (Fig. S1D). The pattern is indexed to confirm the cubic crystal structure, and the *d*-spacings calculated from the pattern are in good agreement with the XRD data. High resolution-transmission electron microscopy (HR-TEM) image shows that {100} crystal planes are exposed on the surfaces of $SrTiO_3$ NCs (Fig. S2). The synthesized and commercial samples are composed of single-crystal $SrTiO_3$ NCs with the {100} facets and irregular shaped $SrTiO_3$ NPs, respectively. The specific surface area was determined to be 19.8 $m^2 g^{-1}$ for $SrTiO_3$ NPs and 9.41 $m^2 g^{-1}$ for $SrTiO_3$ NCs by the BET method.

Au NPs were loaded on $SrTiO_3$ NPs and NCs by the deposition precipitation method using urea as a neutralizer (ESI). The loading amount of Au was quantified to be 3.36 mass% for $Au/SrTiO_3$ NPs and 2.32 mass% for $SrTiO_3$ NCs by inductively coupled plasma spectroscopy. TEM images (Fig. 1, Fig. S3) of $Au/SrTiO_3$ NPs (A) and $Au/SrTiO_3$ NCs (B) show that Au NPs with mean sizes (d_{Au}) of 4.9 nm (C) and 5.1 nm (D) are highly

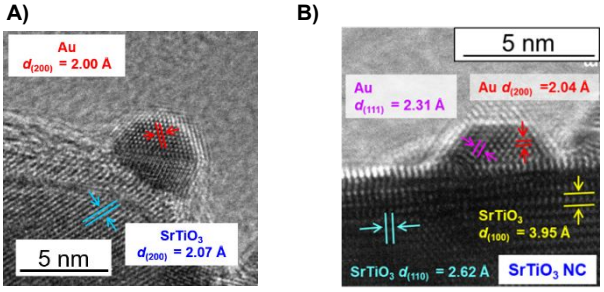

Fig. 2. HR-TEM images of $Au/SrTiO_3$ NP (A) and $Au//SrTiO_3$ NC (B).

dispersed on $SrTiO_3$ NPs and $SrTiO_3$ NCs, respectively. Also, the mean surface-to-surface interparticle distances between the nearest neighbour Au NPs is 9.4 ± 2.7 nm for $Au/SrTiO_3$ NCs and 9.8 ± 3.2 nm for $Au/SrTiO_3$ NPs (Fig. S4). Importantly, the shape of Au NPs is strongly affected by the $SrTiO_3$ support, i.e., every Au NP on $SrTiO_3$ NC takes angular shape with sharp edges and corners, while the Au NP on $SrTiO_3$ NP is hemisphere-like. Both Au and $SrTiO_3$ belong to the cubic crystal system, and the unit cell dimensions (*a*) are 4.079 Å for Au and 3.905 Å for $SrTiO_3$. There exists a lattice mismatch ($\{(a_{Au}-a_{SrTiO_3})/ a_{SrTiO_3}\} \times 100$) of +4.46% between Au and $SrTiO_3$ in the bulk states. In the HR-TEM image of $Au/SrTiO_3$ NP, the interface between Au and $SrTiO_3$ is fairly disordered (Fig. 2A). The *d*-spacings of Au NP (2.00 Å) and $SrTiO_3$ (2.07 Å) are close to the values of the bulk Au(200) (2.039 Å) and $SrTiO_3$(200) (1.952 Å), respectively. In the $Au/SrTiO_3$ NC system, the *d*-spacings of Au(red arrow, 2.04 Å), Au(purple arrow, 2.31 Å), and $SrTiO_3$(yellow arrow, 3.95 Å) are in good agreement with the values of the bulk Au(200), Au(111)(2.355 Å), and $SrTiO_3$(100) (3.90 Å) (Fig. 2B). A heteroepitaxial junction is formed with the orientation relation of $SrTiO_3${100}//Au{100} as shown by the interface models (Fig. S5). The wide-scan X-ray photoelectron (XP) spectrum ascertains the cleanliness of the surface (Fig. S6). The same crystal orientation relation was partly observed for $Au/SrTiO_3$ NPs.[19] Evidiently, the heteroepitaxial junction with $SrTiO_3$ induces faceting of Au NPs to yield truncated pyramids < 10 nm with the clean {111} and {001} surfaces.

UV-Vis-NIR absorption spectra of $Au//SrTiO_3$ NC, $Au/SrTiO_3$ NP, $SrTiO_3$ NC, and $SrTiO_3$ NP were measured (Fig. 3A). Unmodified $SrTiO_3$ NP and NC only have absorption at λ < 380 nm, and from the Tauc plot (Fig. S7), the indirect band gap was determined to be 3.26 eV close to the reported value of $SrTiO_3$.[20] In the spectrum of $Au/SrTiO_3$ NP, strong absorption due to the LSPR of Au NPs appears in the visible region with a fairly sharp peak at 567 nm. In contrast, $Au//SrTiO_3$ NC possesses abnormally broad and strong LSPR absorption with the peak shifted to ~1000 nm. SEM images of $Au//SrTiO_3$ NCs show that Au NPs are highly dispersed on $SrTiO_3$, and the interparticle distance between the nearest neighbour Au NPs (~9.4 nm) in the $Au//SrTiO_3$ NC system is too large to induce the plasmonic coupling between the adjacent Au NPs.[21] To gain insight into the origin for the unique optical character of $Au//SrTiO_3$ NCs, three dimensional-finite difference time domain (3D-FDTD) simulations were performed. Au hemisphere (AuHS) and truncated pyramid (AuTP) placed on $SrTiO_3$ slab were employed as the models for $Au/SrTiO_3$ NP and $Au//SrTiO_3$ NC, respectively (Fig. S8). In the simulation, the incident light

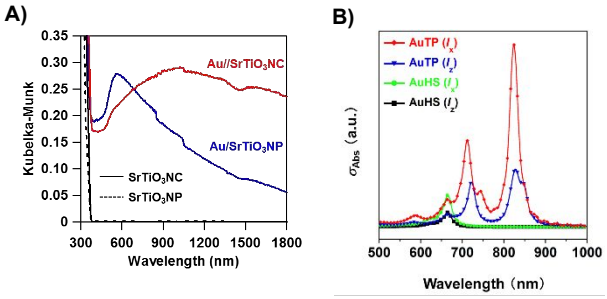

Fig. 3. (A) Absorption spectra of $SrTiO_3$ NP, $SrTiO_3$ NC, $Au/SrTiO_3$ NP, and $Au//SrTiO_3$ NC. (B) Simulated absorption spectra for the models under *y*-polarized light incident from the *z*-axis direction (I_z) and from the x-axis direction (I_x).

with *y*-axis polarization was irradiated on the models from the *z*-axis direction (I_z) or the *x*-axis direction (I_x). In the simulated absorption for $AuTP/SrTiO_3$ and $AuHS/SrTiO_3$ upon the I_z and I_x light irradiation (Fig. 3B), an intense NIR absorption in the spectra for $AuTP/SrTiO_3$ is in good harmony with the experimental spectra. The significant broadening in the experimental spectrum of $Au//SrTiO_3$ NC may be caused by the wide size distribution of Au NPs (Fig. S3B).

The photocatalytic activities of Au/$SrTiO_3$ NP and Au//$SrTiO_3$ NC for OER from an aqueous solution of $AgNO_3$ were studied. Visible-light (λ_{ex} > 400 nm) was irradiated to the catalyst in 10 mM $AgNO_3$ solution with La_2O_3 also added in the solution to maintain the pH during the reaction (pH 7.5) at 298 K. Under these conditions, the Au NP-LSPR is selectively excited since $SrTiO_3$ and La_2O_3 only absorbs UV-light (Fig. S9). In the time courses for O_2 generation (Fig. 4A), the amount of O_2 is expressed by the value per unit mass of catalyst (mol g_{cat}^{-1}). As previously reported, Au/$SrTiO_3$ NP is photocatalytically active for OER (Fig. S10),[11] but the O_2 amount is small at irradiation time (t_p) ≤ 2 h under these conditions. Au//$SrTiO_3$ NC exhibits much higher photocatalytic activity to yield more than 100 μmol g_{cat}^{-1} at t_p = 2 h. All the data were confirmed to be reproducible within the experimental errors less than 12%. The plots of O_2 evolved versus Ag photodeposited on Au//$SrTiO_3$ show a straight line with a slope of ~0.25 (Fig. S11), indicating that the OER stoichiometrically proceeds in the Au//$SrTiO_3$ NC system. To clarify the driving force for the photocataltyic activity of Au//$SrTiO_3$ NC, the apparent quantum yield or external quantum yield (ϕ_{ex}) was measured as a function of λ_{ex} (Fig. 4B, Fig. S12). At λ_{ex} < ~600 nm where the interband transition of Au NPs can occur, the ϕ_{ex} increases with a decrease in λ_{ex} as previously reported.[11] Surprisingly, in the Au//$SrTiO_3$ NC system, even NIR light at 850 nm ≤λ_{ex} ≤ 1200 nm causes OER with a peak ϕ_{ex} of 0.59 ± 0.04% around 750 nm. The similarity of the profiles of the absorption spectrum and action spectrum indicates that the OER is caused by the LSPR excitation of Au NPs on $SrTiO_3$ NCs. The TEM and HR-TEM images, and scanning TEM-energy dispersive spectroscopy (STEM-EDS) line analysis of Au//$SrTiO_3$ NCs after the photocatalytic OER shows that Ag NPs are deposited on the $SrTiO_3$ surface (Fig. S13). Further,

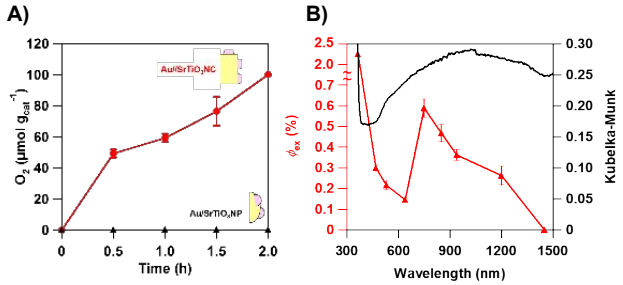

Fig. 4. (A) Time courses for O_2 generation from 10 mM aqueous solution of $AgNO_3$ (10 mL) containing La_2O_3 (20 mg) under visible-light irradiation (λ_{ex} > 400 nm, light intensity = 38 mW cm^{-2}) in the presence of Au/$SrTiO_3$ NP or Au//$SrTiO_3$ NC (10 mg). (B) The action spectrum of external quantum yield (ϕ_{ex}) for the Au//$SrTiO_3$ NC-photocatalyzed OER, and the absorption spectrum of Au//$SrTiO_3$ NC for comparison.

photodeposition of cobalt oxide (CoO_x) was carried out to specify the oxidation sites of Au//$SrTiO_3$ NCs.[18] HR-TEM image shows that nanocrystal identified as Co_3O_4 by the (400) *d*-spacing (2.02 Å) is deposited near the interface between Au nanopyramid and $SrTiO_3$ NC (Fig. S14). Thus, the LSPR excitation of Au//$SrTiO_3$ NCs is followed by the hot-electron transfer from Au NP to $SrTiO_3$ deriving OER on the Au NP surface and Ag^+ reduction on the $SrTiO_3$ surface. In photoelectrochemical cells using a quasi-hemisphere Au/$SrTiO_3$(100) electrode[22] and a quasi-hemisphere Au/TiO_2 electrode modified with CoO_x,[23] high incident photon-to-current conversion efficiencies of ~0.6% and ~0.7% at 580 nm have recently been achieved, respectively, although the values are below 0.1% at $\lambda_{ex} \geq$ 750 nm.

The action mechanism of the Au//$SrTiO_3$ NC-photocatalyzed OER is discussed on the basis of the energy diagram with a Schottky barrier (Scheme S1).[24] When Au NP comes into contact with $SrTiO_3$ in the dark, the interfacial electron transfer from the latter to the former occurs to reach the equilibrium at which both Fermi energies (E_F) are equal. As a result, in the Au//$SrTiO_3$NC(d_{STO} = 180 nm) system, a Schottky barrier of ~0.3 eV can be formed in $SrTiO_3$ near the interface with Au NPs in the same manner as the Au NP-bulk $SrTiO_3$ system.[25] Here we assumed that the flatband potential of $SrTiO_3$ is approximately equal to its CB minimum (E_{CBM} ≈ -4.0 eV).[22] The E_F of Au//$SrTiO_3$ NC is located around -4.3 eV much higher than the E_F of Au in an isolated state (-5.31 eV).[26] Ag^+ ions are adsorbed on the $SrTiO_3$ surface of Au//$SrTiO_3$ NCs in the near-neutral aqueous solution since the point of zero charge is 2.4.[27] According to the energy diagram, plasmonic OER occurs via the Au interband transition needing irradiation by the photons with $\hbar\omega$ > 2.5 eV or λ_{ex} < 500 nm (= E_{CBM}($SrTiO_3$) - *E*(Au *d*-band edge), which is near the value reported for the Au/$SrTiO_3$ NP system.[11] In the Au//$SrTiO_3$ NC system, the hot electrons can be efficiently injected into the CB of $SrTiO_3$ through the high-quality and large area interface (*efficient hot-electron injection*),[28] and the efficient charge separation can be achieved by the Schottky barrier (*effective charge separation*). The electrons transferred to $SrTiO_3$ reduce the adsorbed Ag^+ ions to deposit Ag particles on the surface since they have an energy sufficient for the reduction of Ag^+ ions (standard potential energy, -eU^0(Ag^+/Ag) = -5.24 eV). On the other hand, the hot holes are collected and accumulated near the interfaces between Au NPs and $SrTiO_3$ by the Schottky barrier, which also rationalizes a recent finding that the plasmonic OER takes place at the Au NP/semiconductor interface.[29] Also, the OER can be induced via the intraband transition with the LSPR decay[30] by irradiation of the photons with $\hbar\omega$ = 1.26 eV (= E_{CBM}($SrTiO_3$) + eU(H_2O/O_2)). If the tunnelling through the Schottky barrier can be permitted, the photon energy threshold is further reduced to ~1 eV close to the onset wavelength of the present OER (~1200 nm, Fig. 4B). In this scheme, the probability of electron injection significantly decreases with lowering photon energy, which explains the increase in the gap between the absorption intensity and ϕ_{ex} in the NIR region (Fig. 4B). Consequently, the high photocatalytic activity of Au//$SrTiO_3$ NC is partly ascribable to the efficient electron injection from Au NPs to the CB of $SrTiO_3$ and the suppression of the back electron transfer by the Schottky barrier.

Next, the reason why the intraband transition mechanism effectively works in the Au//$SrTiO_3$ NC system is considered. The spatial distribution of local electric field was calculated by the 3D-FDTD method for the models of AuHS/$SrTiO_3$ and AuTP/$SrTiO_3$ (Fig. S15). The degree of the enhancement of the local electric field intensity was evaluated by the enhancement factor (EF) defined as EF = $|E|^2$ / $|E_0|^2$, where *E* and E_0 are the local maximum electric field and the amplitude of the electric

field of an incident light, respectively. While the electric fields for AuHS/$SrTiO_3$ are spread along the perimeter circle, the electric fields on the surface of AuTP/$SrTiO_3$ are highly concentrated at the corners and edges near the interface. The EF for AuTP/$SrTiO_3$ (1.01×10^6) is approximately twice as large as the EF for AuHS/$SrTiO_3$ (4.71×10^5) under the *x*-axis light irradiation (I_x). These findings suggest that the corners of Au//$SrTiO_3$ NCs act as an antenna to harvest the visible-to-NIR light by modulating LSPR absorption (*effective light harvesting*). Also, the rate of hot-carrier generation is proportional to the square of the product of *E* and transition dipole moment.[31] The plasmonic hot spots generated at the sharp corners and edges near the interface would greatly increase the rates of hot carrier generation by the intraband transition and the following hot-electron injection into the CB of $SrTiO_3$ (*hot-carrier generation and electron injection enhancement*), while water can effectively undergo four-electron oxidation by the hot holes highly concentrated near the interface with the assistance of the electrocatalytic activity of Au NPs (*surface reaction enhancement*).[14]

Conclusions

Au{100}//$SrTiO_3${100}-oriented heteroepitaxial junction with large-contact area induces the bottom-up formation of clean Au truncated pyramids < 10 nm on single-crystalline $SrTiO_3$ NCs in the deposition precipitation process. The nanohybrids provide an external quantum yield of 0.59% at λ_{ex} = 750 nm for plasmonic OER simultaneously with the extension of the photosensitive wavelength to ~1200 nm. We believe that the present habit-modifier free synthesis of Au truncated nanopyramids with plasmonic and catalytic hot spots can widely contribute to the development of not only Au NP-based photocatalysts and electrodes for the solar-to-chemical conversions but also thermally activated catalytic reactions.

This work was supported by JST Adaptable and Seamless Technology Transfer Program through Target-driven R&D, JSPS KAKENHI Grant-in-Aid for Scientific Research (C) no. 20K05674 and 21K05236, the Futaba Foundation, and Nippon Sheet Glass Foundation for Materials Science and Engineering.

Author Contributions

K.K. conducted catalytst synthesis, characterization, and photocatalytic experiments with S. N., M. F. performed FDTD simulations, and H. T. supervised the experimental work and data analysis.

Conflicts of interest

There are no conflicts to declare.

Notes and references

1 T. Ishida, T. Maruyama, A. Taketoshi and M. Haruta, *Chem. Rev.* 2020, **120**, 464-525.
2 N. Lopez and J. K. Nørskov, *J. Am. Chem. Soc.* 2002, **124**, 11262-11263.
3 W. Zhu, R. Michalsky, Ö. Metin, H. Lv, S. Guo, C. J. Wright, X. Sun, A. A. Peterson and S. Sun, *J. Am. Chem. Soc.* 2013, **135**, 16833-16836.
4 L. Kesavan, r. Tiruvalam, M. H. Ab Rahim, M. Z. bin Saiman, D. I. Enache, R. L. Jenkins, N. Dimitratos, J. A. Lopez-Sanchez, S. H. Taylor, D. W. Knight, C. I. Kiely and G. J. Hutchings, *Science* 2011, **331**, 195-199.
5 P. Alexandridis, *Chem. Eng. Technol.* 2011, **34**, 15-28.
6 P. Zhao, N. Li and D. Astruc, *Coord. Chem. Rev*. 2013, **257**, 638-665.
7 Y. Shi, Z. Lyu, M. Zhao, R. Chen, Q. N. Nguyen and Y. Xia, *Chem. Rev*. 2021, **121**, 649-735.
8 M. L. Brongersma, N. J. Halas and P. Nordlander, *Nat. Nanotechnol.* 2015, **10**, 25-34.
9 Y. Tian and T. Tatsuma, *J. Am. Chem. Soc.* 2005, **127**, 7632-7637.
10 A. Furube, L. Du, K. Hara, R. Katoh and M. Tachiya, *J. Am. Chem. Soc.* 2007, **129**, 14852-14853.
11 L. Liu, P. Li, B. Adisak, S. Ouyang, N. Umezawa, J. Ye, R. Kodiyath, T. Tanabe, G. V. Ramesh, S. Ueda and H. Abe, *J. Mater. Chem. A* 2014, **2**, 9875-9882.
12 H. Tada, *Nanoscale Adv.* 2019, **1**, 4238-4245.
13 C. G. Silva, R. Juárez, T. Marino, R. Molinari and H. García, *J. Am. Chem. Soc.* 2011, **133**, 595-602.
14 M. Teranishi, M. Wada, S. Naya and H. Tada, *ChemPhysChem* 2016, **17**, 2813-2817.
15 Y. Nishijima, K. Ueno, Y., Kotake, K. Murakoshi, H. Inoue and H. Misawa, *J. Phys. Chem. Lett*. 2012, **3**, 1248-1252.
16 S. Mubeen, J. Lee, N. Singh, S. Krämer, G. D. Stucky and M. Moskovits, *Nat. Nanotech.* 2013, **8**, 247-251.
17 K. Kimura, S. Naya, Y. Jin-nouchi and H. Tada, *J. Phys. Chem. C* 2012, **116**, 7111-7117.
18 Z. Zheng, N. Murakami, J. Liu, Z. Teng, Q. Zhang, Y. Cao, H. Cheng and T. Ohno, *ChemCatChem* 2020, **12**, 3783-3792.
19 T. Akita and Y. Maeda, *Catal. Lett.* 2018, **148**, 3035-3041.
20 S. Burnside, J. E. Moser, K. Brooks, M. Grätzel and D. Cahen, *J. Phys. Chem. B* 1999, **103**, 9328-9332.
21 T. Kawasaki, Y. Takahashi and T. Tatsuma, *J. Phys. Chem. C* 2013, **117**, 5901-5907.
22 X. Shi, X. Li, T. Toda, T. Oshikiri, K. Ueno, K. Suzuki, M. Murakoshi and H. Misawa, *ACS Appl. Energy Mater*. 2020, **3**, 5675-5683.
23 M. Okazaki, Y. Suganami, N. Hirayama, H. Nakata, T. Oshikiri, T. Yokoi, H. Misawa and K. Maeda, *ACS Appl. Energy Mater.* 2020, **3**, 5142-5146.
24 M. W. Knight, Y. Wang, A. S. Urban, A. Sobhani, B. Zheng, P. Nordlander and N. J. Halas, *Nano Lett*. 2013, **13**, 1687-1692.
25 K. Mitsuhara, Y. Kitsudo, H. Matsumoto, A. Visikovskiy, M. Takizawa, T. Nishimura, T. Akita and Y. Kido, *Surf. Sci.* 2010, **604**, 548-554.
26 D. R. Lide Chief-in-Ed., *Handbook of Chemistry and Physics* 83th Ed., CRC Press, New York, **2002**-**2003**.
27 A. D. Polli, T. Wagner and M. Rühle, *Surf. Sci.* 1999, **429**, 237-245.
28 S. Naya, T. Kume, R. Akashi, M. Fujishima and H. Tada, *J. Am. Chem. Soc.* 2018, **140**, 1251-1254.
29 S. Wang, Y. Gao, S. Miao, T. Liu, L. Mu, R. Li, F. Fan and C. Li, *J. Am. Chem. Soc.* 2017, **139**, 11771-11778.
30 R. Sundararaman, P. Narang, A. S. Jermyn, W. A. Goddard III and H. A. Atwater, *Nat. Commun.* 2014, **5**, 5788.
31 P. Atkins, J. de Paula. *Physical Chemistry*, Eighth Ed., Oxford University Press., Oxford, **2006**.